Direction Selectivity in Naturalistic Action Observation: Distributed Representations Across the Action Observation Network

Zelal Eltaş [1,3], Murat B. Tunca [1,3,4], Burcu A. Urgen [1,2,3]

[1] Department of Neuroscience, Bilkent University, Ankara, Turkey

[2] Department of Psychology, Bilkent University, Ankara, Turkey

[3] Aysel Sabuncu Brain Research Center and National Magnetic Resonance Research Center (UMRAM), Bilkent University, Ankara, Turkey

[4] Department of Mathematics and Computer Science, Physics, Geography, Justus Liebig-Universität Gießen, Gießen, Germany

Author Information

Zelal Eltaş https://orcid.org/0009-0001-6668-0905

Murat B. Tunca https://orcid.org/0000-0002-1597-812X

Burcu A. Urgen https://orcid.org/0000-0001-9664-0309

Corresponding author: Zelal Eltaş, Aysel Sabuncu Brain Research Center, Bilkent University, Ankara, 06800, Turkey. E-mail address: zelal.eltas@gmail.com

Abstract

Perceiving the direction of observed actions is critical for interpreting intentions and guiding social interaction. While direction selectivity has been extensively studied with simple stimuli such as dots, gratings, or point-light displays (PLDs), little is known about how the brain encodes direction in naturalistic, repetitive actions that are seen frequently in daily life. The present fMRI study investigated direction-selective representations during observation of complex actions performed along three bidirectional dimensions (left-right, up-down, front-back) within a 96-video stimulus set. The brain activity was analyzed using multivariate pattern analysis (MVPA) and multiple regression representational similarity analysis (RSA). MVPA revealed above-chance classification of action direction across occipital, parietal, and motor cortices, with the highest decoding in occipital, primary motor, and somatosensory regions. Crucially, RSA demonstrated that when accounting for low-level and motor features, direction information was still represented in early visual cortex, occipito-temporal areas, parietal regions, and motor-related regions. These findings indicate that action direction is represented across multiple levels of the action observation network (AON), extending from early sensory regions to higher-order parietal and frontal cortices. By using naturalistic, repetitive action videos, this study provides new evidence that the coding of action direction in the human brain is broadly distributed, reflecting the complexity of perceiving actions in everyday life. These findings suggest that direction selectivity is a core feature of the action observation network, linking basic motion processing with higher-level action understanding.

Keywords: Visual perception, direction selectivity, action observation network (AON), action perception, multivariate pattern analysis (MVPA), representational similarity analysis (RSA)

Introduction

Perceiving and interpreting everyday actions is important in terms of social interactions and survival of living beings (Boch et al. 2024). In humans, this ability is especially important because everyday environments are rich and complex, requiring precise discrimination of intentions, actions, objects, and motion (Lesourd et al. 2023). For example, when someone waves, one must recognize that the gesture is directed toward them, understand its social intention, and respond by waving back at the appropriate moment to engage in social interaction. Similarly, if one is chased by a dog, they must understand the intention of the dog, run as fast as they can, and be aware of surrounding objects to avoid colliding with them. This ability, especially perceiving biological motion, is both innate and universal due to its survival importance (Bardi et al. 2011; Kuhlmeier et al. 2010; Simion et al. 2008). In fact, in the literature, a specialized network in humans responsible for action perception and interpretation has been proposed consistently, called the action observation network (AON) (Buccino et al. 2001; Caspers et al. 2010; Grosbras et al. 2012). This network includes occipito-temporal regions such as the middle temporal cortex (MT+) and posterior superior temporal sulcus (pSTS), as well as parietal and frontal areas, including the anterior intraparietal sulcus (aIPS), inferior frontal cortex (IFC), and ventral premotor cortex (Caspers et al. 2010; Grosbras et al. 2012; Lesourd et al. 2023; Urgen & Saygin, 2020). These areas work hierarchically, beginning with early visual regions that extract basic visual features such as orientation and motion direction (V1/V2, MT) and extending to higher-order regions that represent action identity, meaning, and goals (Lerner et al. 2001; Neal & Kilner, 2010; Urgen et al, 2019; Urgen & Saygin, 2020; Thompson & Baccus, 2011).

Within this network, occipito-temporal regions are extensively studied and found to play a central role in more basic motion processing (Snowden & Freeman, 2004; Vaina et al. 2001). This connection is particularly important because a key feature of motion processing is direction selectivity, which has been extensively studied in early visual regions, often using macaque models and simple stimuli such as slits, single spots, or random-dot fields (Albright, 1984; Churchland et al. 2004; Hu et al. 2018; Wang & Movshon, 2015). These studies robustly revealed that there are direction-selective neurons in early visual processing regions, predominantly in MT/V5, V1, and V2 (Albright, 1984; Hu et al. 2018; Livingstone, 1998; Wang & Movshon, 2015). These neurons code motion features such as preferred direction (Albright, 1984), speed and orientation tuning (Wang & Movshon, 2015), and motion contrast sensitivity (Hu et al. 2018). Furthermore, the lateral intraparietal area (LIP) was found to encode the direction of motions according to their category (i.e., matching test and sample stimuli's direction), while MT/V5 neurons were strongly direction selective, independent of their categories (Freedman & Assad, 2006). These results have suggested that whereas MT/V5 encodes motion direction irrespective of context, LIP transforms visual direction selectivity into more abstract representations that reflect the behavioral relevance or meaning of stimuli.

Further studies with humans using neuroimaging techniques have yielded similar results, demonstrating the importance of early visual areas on motion perception (Ajina et al. 2014; Hong et

al. 2012; McKeefry et al. 1997; Prieto et al. 2007; Stoppel et al. 2011). The results of motion and direction studies revealed that V1, V2, V3, V4, and MT/V5 areas showed direction-selective responses, independent of motion types (Ajina et al. 2014; Hong et al. 2012; McKeefry et al. 1997; Prieto et al. 2007). Furthermore, in one of the studies, MT/V5 response was enhanced by increased coherence of the moving dots, and suppressed by decreased coherence of the stimuli (Stoppel et al, 2011). In sum, early visual areas, specifically MT/V5, were found to play an important role in discriminating motion direction in both macaque and human brains.

While these findings highlight the contribution of early visual regions, they rely on low-level stimuli such as dots or gratings, which provide limited insight into how the brain processes more complex, biologically relevant motion. To address this, researchers have often used point-light displays (PLDs). PLDs are created by placing dots on the joints of an actor to demonstrate motion kinematics of actions without carrying any information about actors, such as their gender, race, or appearance (Johansson, 1973). Although PLDs lack complex social information, they capture rich kinematic cues, making them useful for studying biological motion (Mather & West, 1993). A recent study has investigated the decoding of direction and velocity of biological motion, using grasping PLDs (Ziccarelli et al. 2024). PLDs have moved either to the left or to the right to perform a grasping action. The results have suggested that MT/V5, superior parieto-occipital cortex (SPOC), and medial intraparietal sulcus (mIPS) have successfully decoded the direction of grasping (Ziccarelli et al. 2024). Another studies using PLDs have shown that in the direction discrimination of a walker, the extrastriate body area (EBA) encodes the facing direction of the walker, whereas the posterior superior temporal sulcus (pSTS) and MT+ encode the walking direction of the PLDs (Vaina et al. 2001; Vangeneugden et al. 2014). Extending these findings, Grossman et al. (2010) demonstrated that the pSTS also maintains action-specific representations that are invariant to changes in size and viewpoint of PLD walkers, highlighting its role in higher-level action perception.

Nevertheless, although PLDs are useful tools when studying biological motion and action observation, they lack cues other than kinematics in actions; thus, they cause weaker activation in AON compared to real-life action videos (Harrison et al, 2013; Orban & Urgen, 2025). Thus, naturalistic action videos were used in the current study to obtain a better understanding of the working mechanisms of action direction selectivity. In addition, stimuli used in early studies, in both biological motion and motion direction studies, moved unidirectionally to capture the direction-specific patterns better. Yet, the real world contains much richer information and complex motion patterns. For instance, the waving action is a repeated motion to the right and left, whereas traditional direction selectivity studies use PLD actions performed towards a single direction in action studies, or use simple stimuli moving unidirectionally in motion studies. Furthermore, those repetitive bidirectional actions are very common in our daily life, such as rolling a dough (i.e., front-back),

wiping the window (i.e., left-right), or shaking hands (i.e., up-down). To our knowledge, no study has investigated these types of stimuli, so whether the bidirectional actions will be represented in MT+ and pSTS as in early studies, or will be carried onto the higher levels of AON, such as the premotor cortex, remains unclear in the literature.

The current study aims to address this gap with an fMRI study in which participants viewed eight naturalistic action videos performed in three different directions (left-right, front-back, and up-down). Unlike commonly used unidirectional moving dot stimuli in the literature, the action videos in the current study consisted of repetitive movements bidirectionally, offering more ecologically valid and complex stimulus patterns. The current study utilizes multivariate analysis techniques, including Multivariate Pattern Analysis (MVPA) and multiple regression Representational Similarity Analysis (RSA). MVPA was used to identify brain areas involved in decoding action direction. However, because MVPA does not reveal whether the decoding reflects direction information specifically or other correlated factors, RSA was applied to control for low-level and motor-related features and thereby isolate direction-specific information.

By using naturalistic videos and multivariate analysis techniques, this study aims to investigate brain regions involved in direction-selective representations of observed actions.

Methods

Participants

Twenty-seven participants (10 male, 26 right-handed; M_{age} = 23) took part in the study. Their participation was voluntary; they did not receive any compensation. All participants reported normal or corrected-to-normal vision and had no history of neurological disorders. They filled in the fMRI compatibility and consent form prior to the study. Recruitment was conducted via social media platforms. Ethical approval for the study was obtained from the Human Research Ethics Committee of Bilkent University.

Stimuli

A stimulus set consisting of 96 action videos were recorded for the current study. The actions were performed along three movement dimensions: horizontal (left-right), vertical (up-down), and depth (front-back). Each dimension included eight actions, representing two exemplars from each of four naturalistic action clusters (Table 1). To increase stimulus variability, two versions of each action were created by altering either the object, the body part involved, or the tool used. All actions were performed by both male and female actors.

The four action clusters were: (1) object manipulation actions, (2) object manipulation actions with a tool, (3) self-directed actions, and (4) self-directed actions with a tool. The eight actions included shaking an object, stretching an object, painting an object with a brush, wiping an object with a cloth, rubbing oneself, scratching oneself, brushing oneself with a facial cleansing brush, and drying oneself with a cloth (Table 1). Actions were selected based on their ability to be performed repetitively and naturally in each movement dimension to ensure ecological validity.

Objects and tools used in the stimuli included plastic bottles, resistance bands, a cardboard box, a mug, acrylic paints, a brush, and a cloth (Table 1). For self-directed actions, actors either used their bare hands or applied tools such as a facial cleansing brush or cloth.

Table 1. A table showing the action types, action clusters, whether a tool is used while performing the actions, and the two variations of the actions in the study.

Action Name	Action Cluster	Tool Used	Variations
Shaking	Object manipulation	None	Water bottle, cola bottle
Stretching			Yellow resistance band, pink resistance band
Painting	Object manipulation with a tool	Painting brush	Purple acrylic paint, green acrylic paint
Wiping		Cloth	Red mug, cardboard box
Rubbing	Self-directed	None	Forehead area, neck area
Scratching			Forehead area, neck area
Drying	Self-directed with a tool	Cloth	Mouth area, forehead area
Brushing		Facial cleansing brush	Cheek area, forehead area

All videos were filmed against a gray wall and a light yellow table. Only the actor's upper body was visible. Actors maintained a downward gaze toward the table and used their right hand for all actions. Actions were performed while facing the camera directly, with the torso and head aligned with the lens. During filming, object/tool/body part positions were adjusted to suit each movement dimension without changing the torso and face position. For instance, while the front part of the forehead is scratched for the up-down and left-right action, the side of the forehead is used for back-front to represent the depth information clearly.

Each action, with both of its variations, was performed by both male and female actors in all three directions. This resulted in 96 video stimuli in total (8 actions × 2 variations × 2 actors × 3 directions), each lasting 3 seconds.

Experimental Design

Procedure

The experiment was programmed using MATLAB (The MathWorks Inc., 2022) and the Psychtoolbox extension (Brainard, 1997; Pelli, 1997; Kleiner et al, 2007). Participants were informed about the study, experimental setup, and signed consent forms before participating. Prior to the functional scans, a high-resolution 6-minute anatomical scan was applied, followed by the experiment.

The experiment consisted of eight runs, each 8 minutes long and comprising 48 trials. Each trial presented a unique combination of action, direction, and actor. Odd-numbered runs (i.e., 1, 3, 5, 7) featured the first variation of each action; even-numbered runs (i.e., 2, 4, 6, 8) featured the second variation. Thus, the full set of 96 videos was divided evenly across the eight runs, in a way that every combination of action, direction, and actor was seen in a run. Each movement direction was shown 16 times per run, totaling 128 repetitions per participant across the experiment. The full session lasted approximately 70 minutes, including 6 minutes of anatomical scans.

Each run began with a 10-second black fixation cross (i.e., rest), followed by trials (Fig. 1). Each trial started with a black fixation cross displayed for a randomly determined duration between 3 and 5 seconds, which was subsequently followed by a 3-second action video (800 x 450 pixels, 25 FPS). During the video, the fixation cross turned into a white dot for visibility, as actors wore black clothing. To minimize the eye movement of the participants, videos were slightly shifted (i.e., a minimum of 10, a maximum of 150 pixels) on the screen to align the relevant action area (e.g., forehead or object) with the fixation point, consistent with previous work (Urgen et al, 2021). For instance, for the rubbing action, a video is slightly shifted downwards to align the fixation point with the hand position of the actor, while for the painting action, it is shifted upwards towards the box.

After the video, a response screen appeared for 2 seconds. Participants indicated the direction of the movement using a button box with three options: left–right, up–down, or back–front (Fig. 1). Participants responded to text appearing on the left side of the screen (i.e., right-left) with their left thumb, and to text appearing in the center and right of the screen (i.e., up-down, front-back) with their right thumb. No feedback was provided. The response screen remained visible for the full 2 seconds regardless of response time. Each run concluded with another 10-second rest period.

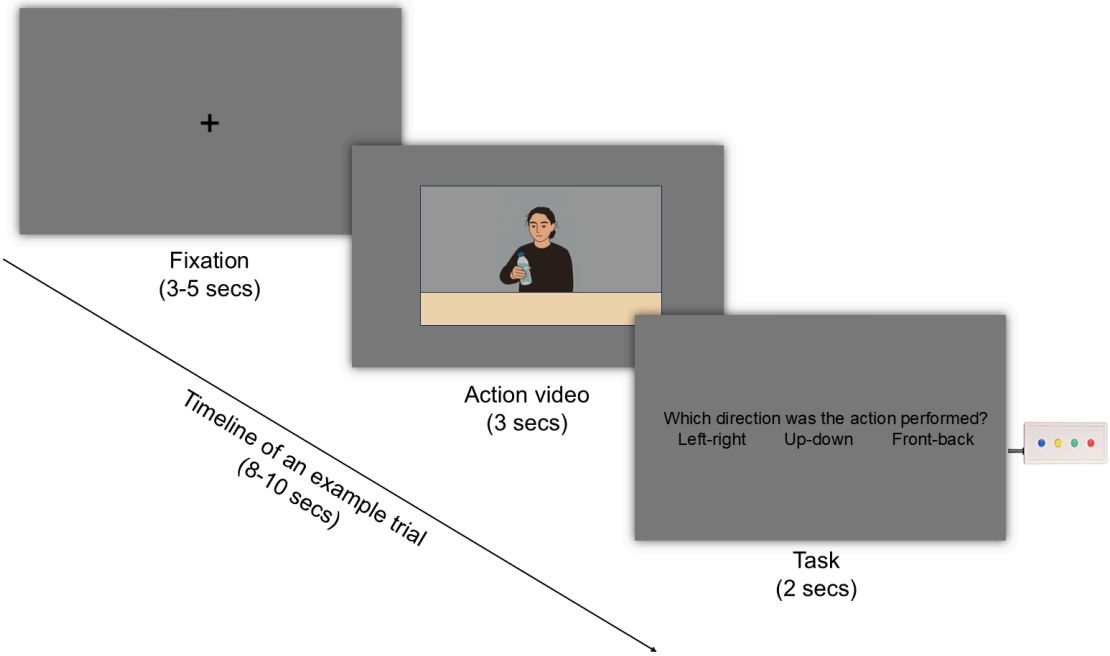

Fig. 1 Example timeline of one trial in the fMRI experiment. Trials began with a fixation cross, followed by an action video and a task requiring participants to indicate the direction of the performed action. Participants gave responses by pressing the buttons on the button box, shown on the right side of the figure. The action video is represented as a drawing for illustrative purposes; the actual study used real action videos.

fMRI Data Acquisition

Data were acquired at the National Magnetic Resonance Research Center (UMRAM) at Bilkent University using a 3T Siemens TimTrio MRI scanner with a 32-channel head coil. Foam cushions were placed around the head, neck, and under the legs to minimize motion. Stimuli were presented on an MR-compatible 32-inch LED monitor (Samsung, 60 Hz refresh rate, 1920x1080 resolution) located 168 cm from the participant's view. A mirror mounted on the head coil allowed participants to view the screen. Prior to functional scanning, a high-resolution T1-weighted

anatomical image was collected (TE = 2.92 ms; TR = 2.6 s; flip angle = 12°; acceleration factor = 2; resolution = 1 mm^3; 176 sagittal slices). Functional images were acquired using EPI sequences (TE = 30 ms; TR = 2 s; flip angle = 90°; FOV = 240 mm; matrix = 96×96; 49 slices; 2.5 mm slice thickness). Each run began with three dummy scans to allow for magnet stabilization.

fMRI Data Analysis

Preprocessing

Anatomical and functional MRI data were preprocessed using fMRIPrep 20.2.6 (Esteban et al. 2018). T1-weighted images were corrected for intensity non-uniformity, skull-stripped, segmented into tissue classes (CSF, white matter, gray matter), and spatially normalized to MNI space. Cortical surface reconstruction was also performed.

Functional runs were motion-corrected, slice-time corrected, co-registered to the anatomical reference, and resampled to both native and standard space. Volumes with excessive motion were identified and marked as outliers. All transformations were applied in a single interpolation step to minimize data degradation. Full details of the preprocessing workflow are available in the fMRIPrep documentation (https://fmriprep.readthedocs.io).

Runs with excessive head motions (translations more than 1.5 mm or rotations more than 1.5°) were excluded from the analysis based on the head motion calculations of fMRIPrep. One participant was excluded from the analysis because of excessive head motions in all runs. Another participant is excluded because of a code malfunction during the fMRI scan. A total of two participants (2 male, 1 left-handed, M_{age} = 23) were excluded from the analysis.

From the remaining twenty-five participants (8M, all right-handed M_{age} = 23), a total of 11 runs were excluded because of head motions: two runs each from three participants and one run each from five participants. One participant's data were collected in two sessions (four runs in each) due to technical problems with the fMRI machine.

Univariate Analyses

Univariate analyses were conducted using the General Linear Model (GLM) implemented in Statistical Parametric Mapping 12 (SPM12; Ashburner et al. 2021) in MATLAB (The MathWorks Inc., 2022). Two separate GLMs were specified to support multivariate analyses. The first GLM was constructed for multivariate pattern analysis (MVPA) and included 12 regressors: 3 action directions (right–left, up–down, front–back), inter-stimulus intervals, response periods, rest periods, and 6

motion parameters (3 translations and 3 rotations). Beta maps of action direction periods were used in decoding analyses.

The second GLM was designed for representational similarity analysis (RSA) and included 105 regressors: 96 action videos, inter-stimulus intervals, response periods, rest periods, and 6 motion parameters (3 translations and 3 rotations). The resulting beta maps for each action video period were used as input for searchlight-based RSA.

Searchlight Multivariate Pattern Analysis (MVPA)

MVPA applies machine learning to fMRI data by training classifiers to detect reproducible spatial activity patterns that distinguish experimental conditions (Mahmoudi et al. 2012). While GLM identifies average activation differences, MVPA allows for the localization of brain regions discriminating between movement directions more sensitively and robustly. The analysis was performed using The Decoding Toolbox (TDT; Hebart et al. 2015) in MATLAB (The MathWorks Inc., 2022). Preprocessed beta images from GLM analysis were used as input. A whole-brain searchlight analysis with a sphere radius of 4 mm was conducted using a linear support vector machine (SVM) classifier and leave-one-run-out cross-validation. Classification was performed across three action directions (right-left, up-down, front-back), and model performance was quantified using accuracy-minus-chance and confusion matrices.

Group-level statistical inference was conducted using threshold-free cluster enhancement (TFCE) with permutation testing, corrected for multiple comparisons, as implemented in CoSMoMVPA (Smith & Nichols, 2009; Oosterhof et al. 2016). Accuracy-minus-chance maps from each subject were entered into a group-level analysis. A TFCE-based Monte Carlo simulation with 10,000 permutations was performed to evaluate the spatial consistency of decoding effects across participants. Z-statistic maps were generated with a correction for multiple comparisons, and a one-tailed threshold of $p < 0.05$ ($z = 1.65$) was applied. The group mean of the accuracy-minus-chance maps was calculated and thresholded with the TFCE map created to obtain significant clusters.

The brain maps were visualized with the BrainNet viewer (Xia et al. 2013). The resulting brain MNI coordinates were labeled by using Automated Anatomical Labelling Atlas 3 (AAL3; Rolls et al. 2020), implemented in MRIcroGL software (Rorden, 2025).

Searchlight Model-based Representational Similarity Analysis

Five model RDMs (Representational Dissimilarity Matrices) were created to identify the hypothesized dissimilarities between action videos. The RDMs were 96x96 in size, representing the pairwise dissimilarities of 96 action videos. The RDMs included three categorical models (direction,

motor response, and action type), one conceptual model (Hierarchical Model and X -HMAX- C1), and one random model (Fig. 2).

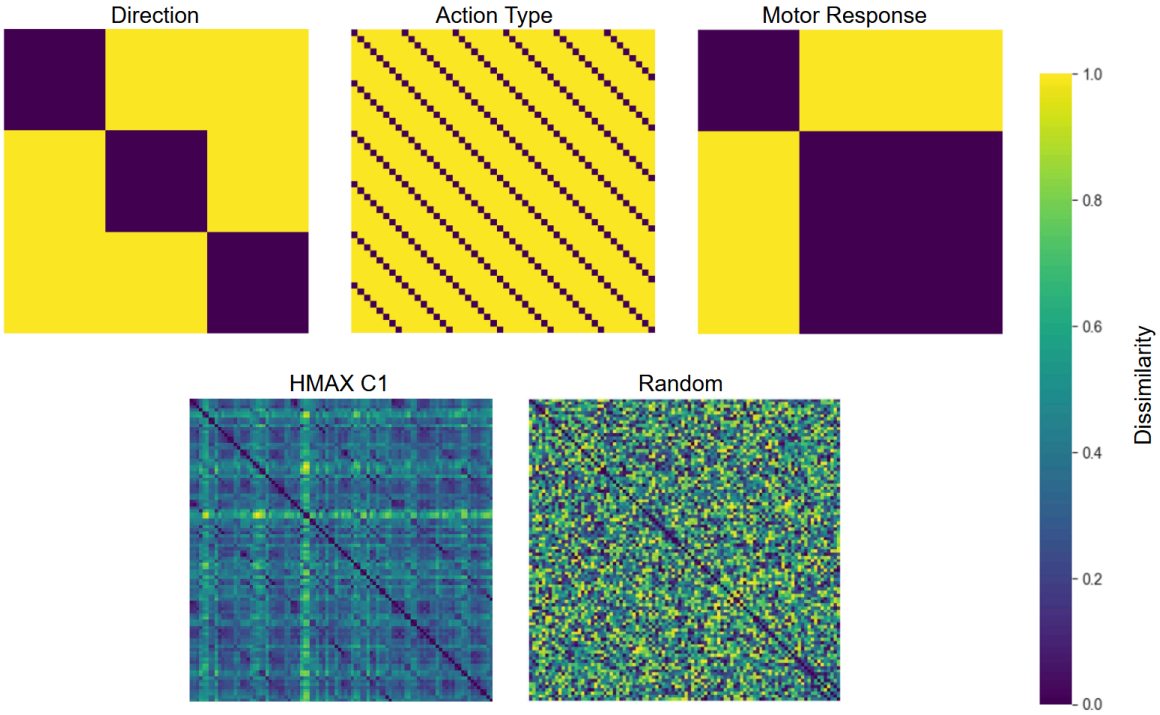

Fig. 2 Five model RDMs used in the RSA: direction, action type, motor response, HMAX C1 and random models. The matrices are 96x96, representing each stimulus pair. 0 indicates that the two stimuli are the same, while 1 indicates that the two stimuli are very different.

The direction model represents the direction in which the action is performed. The action type model represents the actions used in the videos. In the motor response model, the thumb used by participants to respond was coded to eliminate activities related to potential motor preparation. In all three models, a value of 0 indicates that two stimuli belong to the same category, and a value of 1 indicates that they belong to different categories. The fourth and more complex HMAX C1 model is an early-level component of a biologically-inspired visual processing model (Bileschi et al. 2012; Riesenhuber & Poggio, 1999; Serre et al, 2007). It models the low/mid-level features of stimuli (such as edge, shape, color, motion) by imitating complex cell responses at the V1–V2 level in the brain. Data for each stimulus was obtained from this model, the correlation between the data for every two stimuli was calculated, and this was encoded into the dissimilarity matrix using the (1 - correlation) method. A value of 0 indicates that the low/mid-level visual features of the two stimuli are the same, while a value of 1 indicates they are completely different. Finally, the random model was created by generating a random 96x96 matrix in MATLAB, with its diagonal values set to 0 and its second half being the mirror image of the first half. To assess multicollinearity among the representational dissimilarity matrices (RDMs), the Variance Inflation Factor (VIF) for each model was calculated.

Results indicated low risk of multicollinearity for all models (Direction: 1.67, Action: 1.08, Motor: 1.67, HMAX: 1.08, Random: 1.01). These representational dissimilarity matrices (RDMs) were included as input in a multiple regression analysis to determine the unique contribution of each variable in explaining neural patterns, while controlling for the effects of other predictors.Multiple regression representational similarity analysis (RSA) was performed using CoSMoMVPA (Oosterhof et al. 2016). For each subject, beta estimates corresponding to individual action videos obtained from first-level GLM analyses were used to represent condition-specific neural activation patterns. Voxels with zero signal across all samples and any additional non-contributing data were removed for clarity. To control for run-wise variability, data were z-scored within each run. Afterwards, activation patterns for each condition were averaged across runs to achieve a single, stable multivoxel pattern per condition. The resulting dataset was used as input for the representational similarity analysis.

For RSA, a spherical searchlight with a radius of 4 mm was applied across the whole brain to extract local multivoxel patterns. Within each searchlight, a neural representational dissimilarity matrix (RDM) was computed using squared Euclidean distance between activation patterns. This neural RDM was then entered into a multiple regression model, where it was predicted by the aforementioned five model RDMs. The regression was performed locally at each searchlight location, yielding beta maps that reflected the unique contribution of each model in explaining local neural representational structure while accounting for the influence of other predictors.

Regress-out RSA was also conducted to reveal the unique contributions of the direction model, as it was the main research question of the current study. The steps are the same with multiple regression RSA, except this time the direction model was the target model, and the other RDMs were used as regressors.

Group-level statistical inference was conducted using threshold-free cluster enhancement (TFCE) with permutation testing, corrected for multiple comparisons, as implemented in CoSMoMVPA (Oosterhof et al. 2016). For each model, subject-level beta maps from the multiple regression RSA were entered into a one-sample test against zero. A TFCE-based Monte Carlo simulation with 10,000 permutations was performed to assess the spatial consistency of RSA effects across participants. Z-statistic maps were generated for each model, using a one-tailed threshold of $p < 0.05$ ($z = 1.65$). The t-test results were thresholded with the TFCE maps to obtain the significant clusters.

The brain maps were visualized with the BrainNet viewer (Xia et al. 2013). The resulting brain MNI coordinates were labeled by using Automated Anatomical Labelling Atlas 3 (AAL3; Rolls et al. 2020) implemented in MRIcroGL software (Rorden, 2025).

Results

Searchlight Multivariate Pattern Analysis (MVPA)

For the action direction, a three-way searchlight MVPA analysis with a 4 mm spherical radius was performed (Fig. 3). Group-level mean accuracy maps were computed across participants and thresholded with significant clusters obtained from threshold-free cluster enhancement, corrected for multiple comparisons (TFCE; $p < .05$, 10,000 permutations, thresholded at $z = 1.65$). All thresholded areas showed above-chance decoding accuracy (chance level = 33.3%).

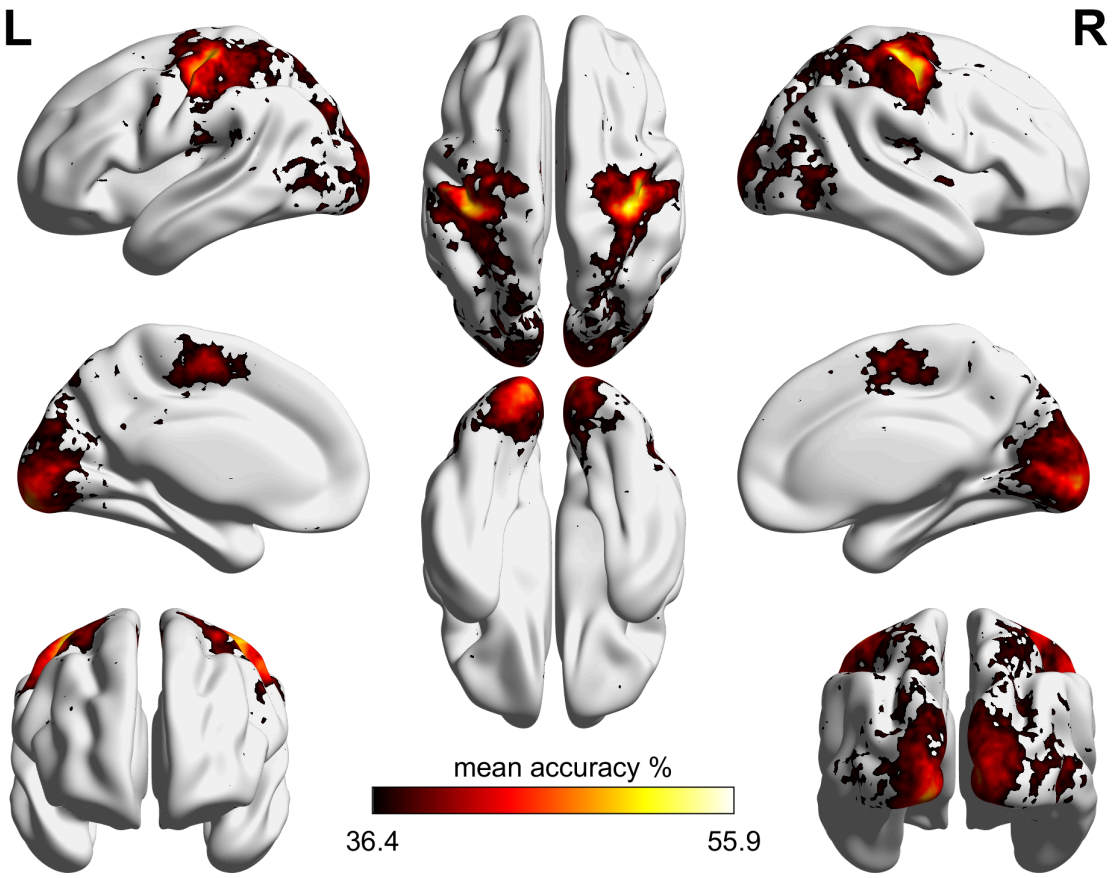

Fig. 3 Group-level mean MVPA decoding accuracy results, thresholded with TFCE-based Monte Carlo simulation with 10,000 permutations ($p < 0.05$, $z = 1.65$). Colorbar shows mean decoding accuracy percentages (chance level = 33.3%). The brain map was visualized using BrainNet (Xia et al, 2013).

The MVPA analysis revealed significant decoding accuracies across a distributed set of occipital, parietal, and motor-related regions (Fig. 3). In the early visual cortex, strong effects were observed bilaterally in the calcarine sulcus (R: 47.6%; L: 45.6%, $p < .001$) and the lingual gyrus (R: 41.1%; L: 43.3%, $p < .001$). Additional occipito-temporal contributions included the superior occipital

gyrus (SOG; R: 39.6%; L: 38.8%, $p < .001$), the inferior occipital gyrus (L IOG: 48.8%, $p < .001$), bilateral middle occipital gyrus (MOG; R: 39.4%; L: 41.2%, $p < .001$), the right lateral occipital cortex (R LOC: 39.4%, $p < .001$), and bilateral MT/V5 (R MT: 41.6%; L MT: 38.3%, $p < .001$).

Parietal regions also showed significant decoding, including the left supramarginal gyrus (40.1%, $p < .001$), bilateral superior parietal lobule (SPL; R: 41.2%; L: 43.3%, $p < .001$), and the left inferior parietal lobule (L IPL: 40.6%, $p < .001$).

In motor-related cortices, robust decoding accuracies were found bilaterally in the precentral gyrus (primary motor cortex, M1; R: 54.8%; L: 50.8%, $p < .001$) and postcentral gyrus (primary somatosensory cortex, S1; R: 48.3%; L: 49.5%, $p < .001$). Significant contributions were also observed in the supplementary motor area (SMA; R: 42.1%; L: 44.1%, $p < .001$).

Overall, these findings demonstrate that direction decoding can be reliably achieved across early visual, occipito-temporal, parietal, and motor cortices, with the highest accuracies observed in sensorimotor regions, particularly the precentral and postcentral gyri. Table 2 presents the peak coordinates of the resulting clusters together with their decoding accuracy percentages and *p*-values thresholded with the TFCE method, corrected for multiple comparisons ($p < .05$, $z = 1.65$).

Table 2. Decoding results of MVPA with peak coordinates, region labels, decoding accuracy percentage, and *p*-values. R: right, L: left, SOG: superior occipital cortex, IOG: inferior occipital gyrus, MOG: middle occipital gyrus, LOC: lateral occipital cortex, MT: middle temporal area (V5), SPL: superior parietal lobule, IPL: inferior parietal lobule, S1: primary somatosensory cortex, M1: primary motor cortex, SMA: supplementary motor area. The labels of the regions were constructed by using the AAL3 atlas.

	MNI Coordinates				
Region (AAL3)	**x**	**y**	**z**	**decoding accuracy %**	***p***
R Calcarine	10	-94	-2	47,6	<.001
L Calcarine	-10	-94	-5	45,6	<.001
R Lingual	13	-77	-5	41,1	<.001
L Lingual	-17	-82	-12	43,3	<.001
R SOG	21	-91	29	39,6	<.001
L SOG	-17	-89	40	38,8	<.001
L IOG	-18	-92	-10	48,8	<.001
R MOG	45	-81	6	39,4	<.001
L MOG	-48	-72	0	41,2	<.001

R LOC	51	-69	-8	39,4	<.001
R MT/V5	48	-58	6	41,6	<.001
L MT/V5	-47	-67	11	38,3	<.001
L Supramarginal	-53	-42	25	40,1	<.001
R SPL	41	-44	62	41,2	<.001
L SPL	-37	-44	65	43,3	<.001
L IPL	-42	-45	56	40,6	<.001
R Postcentral (S1)	38	-27	62	48,3	<.001
L Postcentral (S2)	-39	-27	59	49,5	<.001
R Precentral (M1)	45	16	62	54,8	<.001
L Precentral (M1)	-40	-24	63	50,8	<.001
R SMA	2	-13	60	42,1	<.001
L SMA	-1	14	60	44,1	<.001

Model-based Representational Similarity Analysis

To determine the direction-specific areas by accounting for low-level or motor features, multiple regression RSA with a searchlight radius of 4 mm was conducted. For group-level analysis, a one-sample t-test across the participants was computed and then thresholded with significant clusters obtained from threshold-free cluster enhancement, corrected for multiple comparisons (TFCE; $p < .05$, 10,000 permutations, thresholded at $z = 1.65$). The MNI coordinates and the corresponding regions were taken from the meta-analysis results related to action observation (Caspers et al. 2010).

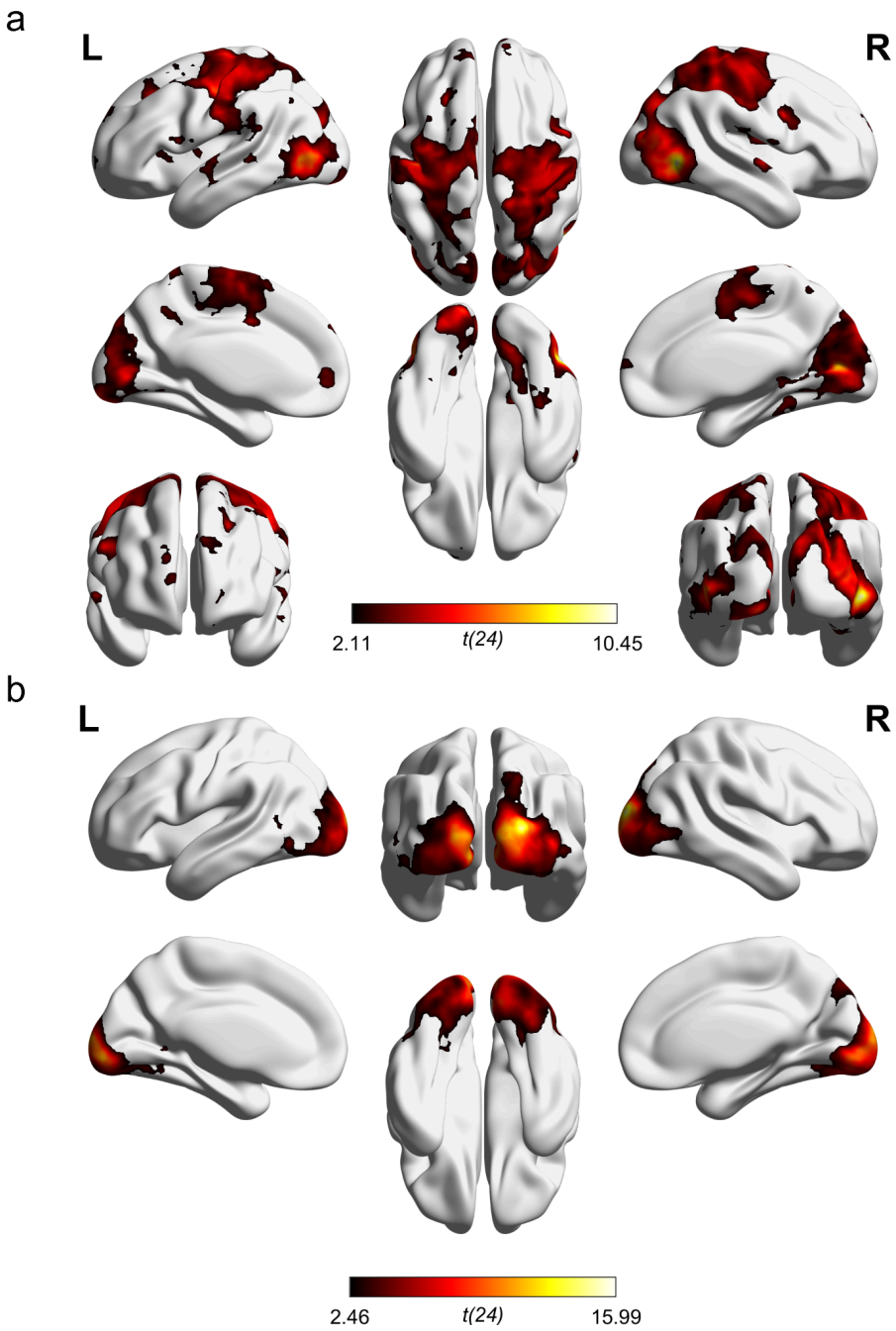

Fig. 4 One-sample t-test multiple regression RSA results, thresholded with TFCE-based Monte Carlo simulation with 10,000 permutations ($p < 0.05$, $z = 1.65$). Colorbar shows t-values. a) Result of the direction model when accounting for HMAX C1, motor, action, and random models. b) Result of the HMAX C1 model when accounting for direction, action, motor, and random models. The brain maps were visualized using BrainNet (Xia et al. 2013).

When accounting for low-level visual (HMAX C1), motor, action, and random models, the direction model revealed significant representational similarity across a broad network of regions (Fig. 4a). In early visual regions, bilateral calcarine sulcus (R: $t(24) = 7.5$; L: $t(24) = 4.5$, $p < .001$) and

lingual gyrus (R: $t(24) = 6.0$; L: $t(24) = 5.3$, $p < .001$) showed robust representation of motion direction. Additional occipital contributions were observed in the middle occipital gyrus (MOG; R: $t(24) = 6.2$; L: $t(24) = 10.0$, $p < .001$) and superior occipital gyrus (SOG; R: $t(24) = 5.5$; L: $t(24) = 4.4$, $p < .001$).

Within occipito-temporal cortex, significant effects were detected in bilateral MT/V5 (R: $t(24) = 9.83$; L: $t(24) = 9.15$, $p < .001$), lateral occipital cortex (LOC; R: $t(24) = 7.3$; L: $t(24) = 5.1$, $p < .001$), and inferior temporal gyrus (ITG; R: $t(24) = 7.9$; L: $t(24) = 7.0$, $p < .001$). Bilateral anterior superior temporal sulcus (aSTS; R: $t(24) = 3.5$; L: $t(24) = 3.9$, $p < .001$) also showed reliable contributions.

In the parietal cortex, direction information was represented in the inferior parietal lobule (R IPL: $t(24) = 4.6$, $p < .001$), and the superior parietal lobule (SPL; L: $t(24) = 4.5$; R: $t(24) = 3.3$, $p < .001$).

Motor-related regions also demonstrated significant involvement in coding direction information. These included the precentral gyrus (primary motor cortex, M1; R: $t(24) = 4.9$; L: $t(24) = 5.5$, $p < .001$), postcentral gyrus (primary somatosensory cortex; R S1: $t(24) = 5.1$; L S2: $t(24) = 4.9$, $p < .001$), and supplementary motor area (SMA; R: $t(24) = 4.2$; L: $t(24) = 4.2$, $p < .001$). Additional contributions were observed in the left dorsal premotor cortex (PMd; BA 6; $t(24) = 4.8$, $p = .012$) and inferior frontal gyrus (IFG; PMv (ventral premotor area); R: $t(24) = 4.0$; L: $t(24) = 2.8$, $p < .001$).

Overall, these results indicate that direction information is represented across a broad cortical network, spanning early visual areas, higher-order occipito-temporal regions, parietal cortex, and motor-related regions, suggesting a distributed representational basis for action direction in the human brain. Table 3 shows the peak MNI coordinates of these regions, their anatomical labeling using the AAL3 atlas, *t*- and *p*-values.

Table 3. The region labels, peak MNI coordinates, *t*- and *p*-values of the results of multiple regression RSA results of the direction model. R: right hemisphere, L: left hemisphere, MOG: middle occipital cortex, SOG: superior occipital cortex, MT: middle temporal area, LOC: lateral occipital cortex, ITG: inferior temporal gyrus, aSTS: anterior superior temporal sulcus, IPL: inferior parietal lobule, SPL: superior parietal lobule, S1: primary somatosensory cortex, M1: primary motor cortex, SMA: supplementary motor area, PMd: dorsal premotor area (Brodmann area 6), IFG: inferior frontal gyrus (PMv, ventral premotor area). The labels of the regions were constructed by using AAL3 atlas.

	MNI Coordinates				
Region (AAL3)	**x**	**y**	**z**	***t*(24)**	***p***
R Calcarine	13	-78	9	7,5	<.001
L Calcarine	-7	-83	9	4,5	<.001
R Lingual	10	-73	4	6	<.001
L Lingual	-6	-78	2	5.3	<.001
R MOG	37	-77	13	6.2	<.001
L MOG	-51	-72	1	10	<.001
R SOG	27	-80	36	5.5	<.001
L SOG	-23	-75	29	4.4	<.001
R MT/V5	48	-64	0	9.83	<.001
L MT/V5	-52	-71	3	9.15	<.001
R LOC	51	-67	-7	7.3	<.001
L LOC	-44	-72	-5	5.1	<.001
R ITG	51	-72	-5	7.9	<.001
L ITG	49	-67	-7	7	<.001
R aSTS	59	-6	1	3.5	<.001
L aSTS	-57	-13	8	3.9	<.001
R IPL	44	-35	45	4.6	<.001
L IPL	-34	-44	52	3.3	<.001
L SPL	-37	-42	57	4.5	<.001
R SPL	22	-62	64	3.3	<.001
R Postcentral (S1)	27	-35	65	5.1	<.001
L Postcentral (S2)	-40	-35	59	4.9	<.001
R Precentral (M1)	40	-23	64	4.9	<.001
L Precentral (M1)	-24	-19	70	5.5	<.001
R SMA	2	-12	54	4.2	<.001

L SMA	-6	-4	58	4.2	<.001
L PMd (BA 6)	-25	24	42	4.8	.012
R IFG (PMv)	54	11	30	4	<.001
L IFG (PMv)	-52	11	16	2.8	<.001

The HMAX C1 model confirmed that the low-level features were successfully represented in the analysis, acting as a baseline (Fig. 4b). The results revealed strong representational similarity effects predominantly in early visual cortex and adjacent occipito-temporal regions. Bilateral calcarine cortex (R: $t(24) = 10.4$; L: $t(24) = 11.1$, $p < .001$) and lingual gyrus (R: $t(24) = 8.5$; L: $t(24) = 8.3$, $p < .001$) showed robust effects. Significant effects were also observed in bilateral superior occipital gyrus (SOG; R: $t(24) = 15.1$; L: $t(24) = 12.9$, $p < .001$) and bilateral middle occipital gyrus (MOG; R: $t(24) = 11.1$; L: $t(24) = 11.0$, $p < .001$).

Beyond early visual regions, the bilateral fusiform gyrus also showed significant effects (R: $t(24) = 7.7$; L: $t(24) = 4.9$, $p < .001$), along with the right cuneus ($t(24) = 4.7$, $p < .001$). In addition, direction-related similarity explained by low-level features was observed in motion-sensitive right MT/V5 ($t(24) = 4.1$, $p < .001$). Finally, effects extended into bilateral inferior temporal gyrus (ITG; R: $t(24) = 3.4$; L: $t(24) = 4.8$, $p < .001$).

Overall, the HMAX C1 model revealed widespread effects across occipital and ventral temporal regions, indicating that low-level visual structure contributes significantly to representational similarity patterns in early and mid-level visual areas. The peak coordinates, *t*-values, and corrected *p*-values thresholded with the TFCE method ($p <.05$, $z = 1.65$) for all clusters are reported in Table 4.

Table 4. The region labels, peak MNI coordinates, *t*- and *p*-values of multiple regression RSA results of the HMAX C1 model. R: right, L: left, SOG: superior occipital cortex, MOG: middle occipital cortex, MT: middle temporal area, ITG: inferior temporal gyrus.

	MNI Coordinates				
Region (AAL3)	**x**	**y**	**z**	***t*(24)**	***p***
R Calcarine	16	-92	4	10,4	<.001
L Calcarine	-7	-92	-3	11,1	<.001
R Lingual	5	-80	-7	8,5	<.001
L Lingual	-8	-87	-9	8,3	<.001
R SOG	23	-96	14	15,1	<.001
L SOG	-9	-103	14	12,9	<.001

R MOG	29	-96	14	11,1	<.001
L MOG	-14	-103	10	11	<.001
R Fusiform	29	-76	-13	7,7	<.001
L Fusiform	-26	-78	-8	4,9	<.001
R Cuneus	21	-80	48	4,7	<.001
R MT/V5	52	-63	-1	4,1	<.001
R ITG	38	-62	-4	3,4	<.001
L ITG	-47	62	-5	4,8	<.001

The results of the action type model also yielded widespread representation in AON, including occipital, occipito-temporal, temporal, motor, parietal, and frontal areas, with the strongest representation in the occipital and occipito-temporal cortices (see Fig. S1 and Table S1 in Supplementary File). On the contrary, for the motor model, only the right calcarine survived in TFCE thresholding (peak MNI coordinates: [18 94 1], $t(24) = 8.3$, $p < .001$), after accounting for action, direction, HMAX and random models. Finally, the random model did not yield any significant clusters in the TFCE thresholded map, as expected ($p > .05$).

Discussion

Although everyday actions are rich in direction information, previous studies have not investigated direction selectivity with naturalistic actions, but have used PLDs and simple moving dots or gratings. The present study addressed this gap by investigating the neural basis of action direction selectivity using naturalistic, repetitive, bidirectional action videos and multivariate fMRI analyses. First, we employed MVPA to identify brain regions that contained sufficient information to discriminate between action directions (i.e., decodability; Peelen & Downing, 2023; Popal et al. 2020). While informative, decoding analysis may conflate direction with correlated features and/or underrepresent certain direction-selective areas (Diedrichsen & Kriegeskorte, 2017; Popal et al. 2020). To address this issue, we then applied multiple regression RSA, which enables testing the unique contribution of direction information after accounting for low-level, motor, and action-related effects (Freund et al. 2021; Popal et al. 2020; Xue et al. 2013). Because RSA directly compares neural similarity matrices with model-derived structures, it offers greater sensitivity and localizes representationally relevant regions more precisely than MVPA (Freund et al. 2021; Weaverdyck et al. 2020). In this framework, MVPA provided a critical baseline by establishing the decodability of action directions, while RSA refined these results by isolating direction-specific representations. Together, these complementary methods allowed us to robustly characterize the neural coding of action direction.

Results have revealed strong decoding and representation of action direction within the action observation network (AON), including occipital, occipito-temporal, parietal, motor, and frontal areas bilaterally. These findings extend prior work on motion perception and biological motion processing, providing novel evidence that action direction is represented not only in low-level sensory regions (i.e., visual cortex and MT), but also in higher-level action-related areas when ecologically valid, naturalistic action stimuli are used.

Consistent with previous studies in macaques and humans, strong direction decoding and representation in early visual regions (i.e., calcarine cortex, lingual area, MOG, SOG, MT/V5) were observed (Albright, 1984; Hong et al. 2012; Stoppel et al. 2011; Vaina et al. 2001; Vangeneugden et al. 2014; Wurm & Erigüç, 2025; Ziccarelli et al. 2024). Additionally, the multiple regression RSA confirmed that these effects could not be explained solely by low-level visual features captured by the HMAX C1 model, suggesting direction-specific neural coding. The involvement of LOC further supports that occipito-temporal areas contribute not only to object and form processing (Eger et al. 2007; Snow et al. 2015) but also to the integration of motion cues relevant for action interpretation (Vaina et al. 2001; Vangeneugden et al. 2014; Weiner & Grill-Spector, 2011). Together, these results suggest that occipito-temporal cortices are essential for encoding direction across a range of visual and action contexts.

Results revealed direction-selective representations within the parietal cortex, specifically in both the inferior parietal lobule (IPL) and the superior parietal lobule (SPL). The IPL is a key multimodal area that integrates visual information with spatial properties, and it has been strongly implicated in action observation and imitation (Caspers et al. 2010; Fogassi & Luppino, 2005). This integrative role makes it a plausible candidate for representing action direction, as accurate interpretation of an observed action often requires linking visual motion cues with their spatial orientation and trajectory (Karnath, 1997). Within the SPL, our findings are consistent with previous work showing that the superior parieto-occipital cortex (SPOC) decodes the movement direction of point-light display (PLD) hand movements using MVPA (Ziccarelli et al. 2024). More broadly, the involvement of intraparietal areas may indicate abstract representations of direction, in line with evidence from both macaque and human studies (Freedman & Assad, 2006; Ziccarelli et al. 2024). Supporting this view, electrophysiological research has shown that the posterior parietal cortex (PPC), which includes the lateral intraparietal area (LIP) and the parietal reach region (PRR), contains neurons tuned to motion direction (Andersen & Buneo, 2002).

Along with parietal regions, results have revealed the motor-related regions robustly for action direction: SMA, premotor, dorsal premotor, primary motor, and primary somatosensory areas. The results of the dorsal premotor cortex are consistent with a previous study that found that the direction of an abstract animation (i.e., right-to-left and left-to-right) was decoded in the right dorsal premotor area and MT/V5 (Wurm & Erigüç, 2025). Moreover, a study on hand movement direction during motor planning and execution reported that SMA and parietal areas are engaged in planning,

whereas motor and premotor cortices decode movement direction during execution (Combrisson et al. 2024). Similarly, in the reaching task (i.e., left or right), direction information was represented within superior parietal and premotor areas (Caceres et al. 2024). Another study involved the wrist and forearm movements of 8 directions and found that the primary motor cortex, supplementary motor area, and premotor cortex were selective to movement directions of the hand (Cowper-Smith et al. 2010). Furthermore, a similar study with wrist movements of monkeys has found that the neurons in the ventral premotor area were directionally tuned independent of the position of the posture of the hand (Kakei et al. 2001). Although these works addressed action execution rather than observation, our findings converge, as action observation and execution are closely linked within overlapping neural circuits, especially in parietal and motor cortices (Culham & Valyegar, 2006; Grezes & Decety, 2001; Vignemont & Haggard, 2008). The current study extends these findings by confirming that similar directional coding emerges during action perception within parietal and motor cortices.

Although previous work has revealed direction selectivity at multiple levels of the action observation network (AON) from low-level visual regions such as V1-V4 and MT/V5 (Albright, 1984; Hong et al. 2012; Stoppel et al. 2011) to higher-order parietal and premotor cortices (Freedman & Assad, 2006; Wurm & Erigüç, 2025; Caceres et al. 2024), these studies have typically highlighted specific regions rather than demonstrating a broad, network-wide representation of direction information. The present study revealed that direction information of complex, bidirectional actions is represented across multiple levels of the action observation network (AON), reflecting the multi-layered nature of perceptual, motor, and cognitive processes involved in interpreting complex actions. Such widespread engagement may be necessary because actions encountered in daily life are rarely simple or unidirectional but instead involve rich spatial dynamics that must be integrated for accurate perception and understanding. Importantly, this study shows that direction selectivity is not restricted to early visual regions, as in the previous visual direction selectivity studies, but higher-order parietal and frontal regions also contribute when the observed actions are more naturalistic and complex, highlighting the multilayered coding of direction within the human brain. These results might suggest that direction information may be represented hierarchically, in early visual regions such as V1/V2 and MT in a sensory manner, and extended into more abstract representations in higher-order areas such as the premotor and PMv, where the direction of actions may be categorically interpreted in terms of their meaning or goal.

Several limitations of the current study should be acknowledged. One limitation concerns the stable positioning of the on-screen texts in our task, which might have accidentally created spatial associations and motor preparation. Although we attempted to compensate for this by including a motor model in the RSA, future studies could minimize such risks by varying or randomizing text locations across trials. Another limitation is that our stimuli were limited to a set of three bidirectional movement dimensions. Using naturalistic actions that are non-repetitive, either bidirectional or

unidirectional, could provide valuable insight into whether the observed representational patterns generalize beyond repetitive trajectories. Similarly, using communicative action stimuli such as waving a hand or handshaking could reveal the processing of directions regarding socially meaningful stimuli. A promising approach would also be to employ more naturalistic, real-world setups combined with EEG recordings, where depth and three-dimensional motion cues can be captured with higher ecological validity and temporal precision. Despite these limitations, the present study offers important insights into the global processing of direction information in the action observation network for complex, repetitive, and naturalistic actions.

Conclusion

The present study provides novel evidence that direction selectivity during naturalistic action observation is not limited to early visual cortices but is broadly distributed across the action observation network. Using complementary multivariate approaches, MVPA and RSA, we demonstrated that direction information is represented in occipital, temporal, parietal, and frontal regions. Importantly, these results extend prior work based on simplified or point-light stimuli by showing that complex, repetitive, and ecologically valid actions demonstrate widespread, global representations of direction.

Taken together, these findings highlight the distributed and integrative nature of direction coding in the human brain, supporting the view that action direction is a fundamental property represented at multiple levels of the action observation network. This broad representation may allow the brain to flexibly interpret action trajectories in naturalistic contexts, bridging low-level motion processing with higher-order action understanding and prediction.

Acknowledgements

The authors would like to thank Ece Altınbaş for her contributions in stimulus conceptualization and creation, and Cenk Günsel for his contributions in stimulus recording. Additionally, the authors appreciate the undergraduate research assistants who helped with fMRI data collection. The authors would also like to thank the Turkish Health Institutes Presidency (TUSEB) for funding this study (Project No: 37734). The preprocessing of the fMRI data was fully performed at TUBITAK ULAKBIM, High Performance and Grid Computing Center (TRUBA resources).

Author Contributions

Zelal Eltaş: Writing – original draft, Investigation, Visualization, Software, Methodology, Formal analysis, Conceptualization, Funding acquisition. **Murat B. Tunca**: Writing – review & editing, Formal analysis, Supervision, Methodology, Conceptualization, Funding acquisition. **Burcu A. Urgen**: Writing – review & editing, Supervision, Methodology, Conceptualization.

Data and Code Availability

Data will be made available upon request. Stimulus set and analysis codes of the current study are available at the Open Science Framework's website at https://osf.io/9sqyd/

References

Ajina, S., Kennard, C., Rees, G., & Bridge, H. (2014). Motion area V5/MT+ response to global motion in the absence of V1 resembles early visual cortex. *Brain*, *138*(1), 164–178. https://doi.org/10.1093/brain/awu328

Albright, T. D. (1984). Direction and orientation selectivity of neurons in visual area MT of the macaque. *Journal of Neurophysiology*, *52*(6), 1106–1130. https://doi.org/10.1152/jn.1984.52.6.1106

Andersen, R. A., & Buneo, C. A. (2002). Intentional maps in posterior parietal cortex. *Annual Review of Neuroscience*, *25*(1), 189–220. https://doi.org/10.1146/annurev.neuro.25.112701.142922

Ashburner, J., Barnes, G. R., Chen, C., & Zeidman, P. (2021). SPM12 Manual. *ResearchGate*. https://www.researchgate.net/publication/355544981_SPM12_Manual

Bardi, L., Regolin, L., & Simion, F. (2010). Biological motion preference in humans at birth: role of dynamic and configural properties. *Developmental Science*, *14*(2), 353–359. https://doi.org/10.1111/j.1467-7687.2010.00985.x

Bileschi, S., Martin, J. G., Riesenhuber, M., Rule, J., & Serre, T. R. (2012). *HMAX: Hierarchical Model and X* [Software]. GitHub. https://github.com/joshrule/hmax

Binkofski, F., & Buccino, G. (2006). The role of ventral premotor cortex in action execution and action understanding. *Journal of Physiology-Paris*, *99*(4–6), 396–405. https://doi.org/10.1016/j.jphysparis.2006.03.005

Boch, M., Karl, S., Wagner, I. C., Lengersdorff, L. L., Huber, L., & Lamm, C. (2024). Action observation reveals a network with divergent temporal and parietal cortex engagement in dogs compared to humans. *Imaging Neuroscience*, *2*, 1–29. https://doi.org/10.1162/imag_a_00385

Brainard, D. H. (1997). The Psychophysics toolbox. *Spatial Vision*, *10*(4), 433–436. https://doi.org/10.1163/156856897x00357

Buccino, G., Binkofski, F., Fink, G. R., Fadiga, L., Fogassi, L., Gallese, V., Seitz, R. J., Zilles, K., Rizzolatti, G., & Freund, H. (2001). Action observation activates premotor and parietal areas in a somatotopic manner: an fMRI study. *European Journal of Neuroscience*, *13*(2), 400–404. https://doi.org/10.1111/j.1460-9568.2001.01385.x

Caceres, A. H., Barany, D. A., Dundon, N. M., Smith, J., & Marneweck, M. (2024). Neural encoding of direction and distance across reference frames in visually guided reaching. *eNeuro*, *11*(12), ENEURO.0405-24.2024. https://doi.org/10.1523/eneuro.0405-24.2024

Caspers, S., Zilles, K., Laird, A. R., & Eickhoff, S. B. (2010). ALE meta-analysis of action observation and imitation in the human brain. *NeuroImage*, *50*(3), 1148–1167. https://doi.org/10.1016/j.neuroimage.2009.12.112

Churchland, M. M., Priebe, N. J., & Lisberger, S. G. (2004). Comparison of the spatial limits on direction selectivity in visual areas MT and V1. *Journal of Neurophysiology*, *93*(3), 1235–1245. https://doi.org/10.1152/jn.00767.2004

Combrisson, E., Di Rienzo, F., Saive, A., Perrone-Bertolotti, M., Soto, J. L. P., Kahane, P., Lachaux, J., Guillot, A., & Jerbi, K. (2024). Human local field potentials in motor and non-motor brain areas encode upcoming movement direction. *Communications Biology*, *7*(1). https://doi.org/10.1038/s42003-024-06151-3

Cowper-Smith, C. D., Lau, E. Y. Y., Helmick, C. A., Eskes, G. A., & Westwood, D. A. (2010). Neural coding of movement direction in the healthy human brain. *PLoS ONE*, *5*(10), e13330. https://doi.org/10.1371/journal.pone.0013330

Culham, J. C., & Valyear, K. F. (2006). Human parietal cortex in action. *Current Opinion in Neurobiology*, *16*(2), 205–212. https://doi.org/10.1016/j.conb.2006.03.005

Diedrichsen, J., & Kriegeskorte, N. (2017). Representational models: A common framework for understanding encoding, pattern-component, and representational-similarity analysis. *PLoS Computational Biology*, *13*(4), e1005508. https://doi.org/10.1371/journal.pcbi.1005508

Eger, E., Ashburner, J., Haynes, J., Dolan, R. J., & Rees, G. (2007). fMRI Activity Patterns in Human LOC Carry Information about Object Exemplars within Category. *Journal of Cognitive Neuroscience*, *20*(2), 356–370. https://doi.org/10.1162/jocn.2008.20019

Esteban, O., Markiewicz, C., Blair, R., Moodie, C., Isik, A. I., Erramuzpe, A., Kent, J. D., Goncalves, M., DuPre, E., Snyder, M., Oya, H., Ghosh, S., Wright, J., Durnez, J., Poldrack, R. A., & Gorgolewski, K. J. (2018). fMRIPrep: a robust preprocessing pipeline for functional MRI. *Nature Methods*, *16*(1), 111–116. https://doi.org/10.1038/s41592-018-0235-4

Fogassi, L., & Luppino, G. (2005). Motor functions of the parietal lobe. *Current Opinion in Neurobiology*, *15*(6), 626–631. https://doi.org/10.1016/j.conb.2005.10.015

Freedman, D. J., & Assad, J. A. (2006). Experience-dependent representation of visual categories in parietal cortex. *Nature*, *443*(7107), 85–88. https://doi.org/10.1038/nature05078

Freund, M. C., Etzel, J. A., & Braver, T. S. (2021). Neural coding of cognitive control: the representational similarity analysis approach. *Trends in Cognitive Sciences*, *25*(7), 622–638. https://doi.org/10.1016/j.tics.2021.03.011

Grèzes, J., & Decety, J. (2001). Functional anatomy of execution, mental simulation, observation, and verb generation of actions: a meta-analysis. *Human brain mapping*, *12*(1), 1–19. 10.1002/1097-0193(200101)12:1<1::aid-hbm10>3.0.co;2-v

Grosbras, M., Beaton, S., & Eickhoff, S. B. (2011). Brain regions involved in human movement perception: A quantitative voxel‐based meta‐analysis. *Human Brain Mapping*, *33*(2), 431–454. https://doi.org/10.1002/hbm.21222

Grossman, E. D., Jardine, N. L., & Pyles, J. A. (2010). fMR-adaptation reveals invariant coding of biological motion on human STS. *Frontiers in Human Neuroscience*. https://doi.org/10.3389/neuro.09.015.2010

Harrison, R. E., Giesel, M., & Hesse, C. (2023). Action perception in athletes: Expertise facilitates perceptual discrimination. *Perceptual and Motor Skills*, *130*(4), 1472–1494. https://doi.org/10.1177/00315125231182046

Hebart, M. N., Gorgen, K., & Haynes, J. (2015). The Decoding Toolbox (TDT): a versatile software package for multivariate analyses of functional imaging data. *Frontiers in Neuroinformatics*, *8*. https://doi.org/10.3389/fninf.2014.00088

Hong, S. W., Tong, F., & Seiffert, A. E. (2011). Direction-selective patterns of activity in human visual cortex suggest common neural substrates for different types of motion. *Neuropsychologia*, *50*(4), 514–521. https://doi.org/10.1016/j.neuropsychologia.2011.09.016

Hu, J., Ma, H., Zhu, S., Li, P., Xu, H., Fang, Y., Chen, M., Han, C., Fang, C., Cai, X., Yan, K., & Lu, H. D. (2018). Visual motion processing in macaque V2. *Cell Reports*, *25*(1), 157-167.e5. https://doi.org/10.1016/j.celrep.2018.09.014

Johansson, G. (1973). Visual perception of biological motion and a model for its analysis. *Perception & Psychophysics*, *14*(2), 201–211. https://doi.org/10.3758/bf03212378

Kakei, S., Hoffman, D. S., & Strick, P. L. (2001). Direction of action is represented in the ventral premotor cortex. *Nature Neuroscience*, *4*(10), 1020–1025. https://doi.org/10.1038/nn726

Karnath, H. (1997). Spatial orientation and the representation of space with parietal lobe lesions. *Philosophical Transactions of the Royal Society B Biological Sciences*, *352*(1360), 1411–1419. https://doi.org/10.1098/rstb.1997.0127

Kleiner M, Brainard D, Pelli D. (2007). "What's new in Psychtoolbox-3?" *Perception 36 ECVP Abstract Supplement*. https://doi.org/10.1177/03010066070360S101

Kuhlmeier, V. A., Troje, N. F., & Lee, V. (2010). Young infants detect the direction of biological motion in Point‐Light displays. *Infancy*, *15*(1), 83–93. https://doi.org/10.1111/j.1532-7078.2009.00003.x

Lerner, Y., Hendler, T., Ben-Bashat, D., Harel, M., & Malach, R. (2001). A hierarchical axis of object processing stages in the human visual cortex. *Cerebral Cortex*, *11*(4), 287–297. https://doi.org/10.1093/cercor/11.4.287

Lesourd, M., Afyouni, A., Geringswald, F., Cignetti, F., Raoul, L., Sein, J., Nazarian, B., Anton, J., & Grosbras, M. (2023). Action observation network activity related to object-directed and socially-directed actions in adolescents. *Journal of Neuroscience*, *43*(1), 125–141. https://doi.org/10.1523/jneurosci.1602-20.2022

Livingstone M. S. (1998). Mechanisms of direction selectivity in macaque V1. *Neuron*, *20*(3), 509–526. https://doi.org/10.1016/s0896-6273(00)80991-5

Mahmoudi, A., Takerkart, S., Regragui, F., Boussaoud, D., & Brovelli, A. (2012). Multivoxel pattern analysis for fMRI data: A review. *Computational and Mathematical Methods in Medicine*, *2012*, 1–14. https://doi.org/10.1155/2012/961257

Mather, G., & West, S. (1993). Recognition of animal locomotion from dynamic point-light displays. *Perception*, *22*(7), 759–766. https://doi.org/10.1068/p220759

The MathWorks Inc. (2022). MATLAB version: 9.12.0 (R2022a), Natick, Massachusetts: The MathWorks Inc. https://www.mathworks.com

McKeefry, D., Watson, J., Frackowiak, R., Fong, K., & Zeki, S. (1997). The Activity in Human Areas V1/V2, V3, and V5 during the Perception of Coherent and Incoherent Motion. *NeuroImage*, *5*(1), 1–12. https://doi.org/10.1006/nimg.1996.0246

Neal, A., & Kilner, J. M. (2010). What is simulated in the action observation network when we observe actions? *European Journal of Neuroscience*, *32*(10), 1765–1770. https://doi.org/10.1111/j.1460-9568.2010.07435.x

Oosterhof, N. N., Tipper, S. P. & Downing, P. E. (2013). Crossmodal and action-specific: neuroimaging the human mirror neuron system. Trends in Cognitive Sciences, 17(7), 311-318. https://doi.org/10.1016/j.tics.2013.04.012

Orban, G. A., & Urgen, B. A. (2025). Functional imaging of the human visual system. In M. Filippi (Ed.), *fMRI techniques and protocols* (vol. 220, pp. 597–631). Neuromethods. https://doi.org/10.1007/978-1-0716-4438-6_19

Peelen, M. V., & Downing, P. E. (2023). Testing cognitive theories with multivariate pattern analysis of neuroimaging data. *Nature Human Behaviour*, *7*(9), 1430–1441. https://doi.org/10.1038/s41562-023-01680-z

Pelli, D. G. (1997). The VideoToolbox software for visual psychophysics: transforming numbers into movies. *Spatial Vision*, *10*(4), 437–442. https://doi.org/10.1163/156856897x00366

Popal, H., Wang, Y., & Olson, I. R. (2020). A Guide to representational similarity analysis for social neuroscience. *Social Cognitive and Affective Neuroscience*, *14*(11), 1243–1253. https://doi.org/10.1093/scan/nsz099

Prieto, E. A., Barnikol, U. B., Soler, E. P., Dolan, K., Hesselmann, G., Mohlberg, H., Amunts, K., Zilles, K., Niedeggen, M., & Tass, P. A. (2007). Timing of V1/V2 and V5+ activations during coherent motion of dots: An MEG study. *NeuroImage*, *37*(4), 1384–1395. https://doi.org/10.1016/j.neuroimage.2007.03.080

Riesenhuber, M., & Poggio, T. (1999). Hierarchical models of object recognition in cortex. *Nature Neuroscience*, *2*(11), 1019–1025. https://doi.org/10.1038/14819

Rolls, E. T., Huang, C., Lin, C., Feng, J., & Joliot, M. (2019). Automated anatomical labelling atlas 3. *NeuroImage*, *206*, 116189. https://doi.org/10.1016/j.neuroimage.2019.116189

Rorden, C. (2025). MRIcroGL: voxel-based visualization for neuroimaging. *Nature Methods*. https://doi.org/10.1038/s41592-025-02763-7

Serre, T., Kreiman, G., Kouh, M., Cadieu, C., Knoblich, U., & Poggio, T. (2007). A quantitative theory of immediate visual recognition. *Progress in Brain Research*, 33–56. https://doi.org/10.1016/s0079-6123(06)65004-8

Simion, F., Regolin, L., & Bulf, H. (2008). A predisposition for biological motion in the newborn baby. *Proceedings of the National Academy of Sciences*, *105*(2), 809–813. https://doi.org/10.1073/pnas.0707021105

Smith, S., & Nichols, T. (2008). Threshold-free cluster enhancement: Addressing problems of smoothing, threshold dependence and localisation in cluster inference. *NeuroImage*, *44*(1), 83–98. https://doi.org/10.1016/j.neuroimage.2008.03.061

Snow, J. C., Goodale, M. A., & Culham, J. C. (2015). Preserved haptic shape processing after bilateral LOC lesions. *Journal of Neuroscience*, *35*(40), 13745–13760. https://doi.org/10.1523/jneurosci.0859-14.2015

Snowden, R. J., & Freeman, T. C. (2004). The visual perception of motion. *Current Biology*, *14*(19), R828–R831. https://doi.org/10.1016/j.cub.2004.09.033

Stoppel, C. M., Boehler, C. N., Strumpf, H., Heinze, H., Noesselt, T., Hopf, J., & Schoenfeld, M. A. (2011). Feature‐based attention modulates direction‐selective hemodynamic activity within human MT. *Human Brain Mapping*, *32*(12), 2183–2192. https://doi.org/10.1002/hbm.21180

Thompson, J. C., & Baccus, W. (2011). Form and motion make independent contributions to the response to biological motion in occipitotemporal cortex. *NeuroImage*, *59*(1), 625–634. https://doi.org/10.1016/j.neuroimage.2011.07.051

Urgen, B. A., & Orban, G. A. (2021). The unique role of parietal cortex in action observation: Functional organization for communicative and manipulative actions. *NeuroImage*, *237*, 118220. https://doi.org/10.1016/j.neuroimage.2021.118220

Urgen, B. A., & Saygin, A. P. (2020). Predictive processing account of action perception: Evidence from effective connectivity in the action observation network. *Cortex*, *128*, 132–142. https://doi.org/10.1016/j.cortex.2020.03.014

Urgen, B. A., Pehlivan, S., & Saygin, A. P. (2019). Distinct representations in occipito-temporal, parietal, and premotor cortex during action perception revealed by fMRI and computational modeling. Neuropsychologia, 127, 35–47. https://doi.org/10.1016/j.neuropsychologia.2019.02.006

Vaina, L. M., Solomon, J., Chowdhury, S., Sinha, P., & Belliveau, J. W. (2001). Functional neuroanatomy of biological motion perception in humans. *Proceedings of the National Academy of Sciences*, *98*(20), 11656–11661. https://doi.org/10.1073/pnas.191374198

Vangeneugden, J., Peelen, M. V., Tadin, D., & Battelli, L. (2014). Distinct neural mechanisms for body form and body motion discriminations. *Journal of Neuroscience*, *34*(2), 574–585. https://doi.org/10.1523/jneurosci.4032-13.2014

Vignemont, F., & Haggard, P. (2008). Action observation and execution: What is shared? *Social Neuroscience*, *3*(3–4), 421–433. https://doi.org/10.1080/17470910802045109

Weaverdyck, M. E., Lieberman, M. D., & Parkinson, C. (2020). Tools of the trade multivoxel pattern analysis in fMRI: a practical introduction for social and affective neuroscientists. *Social Cognitive and Affective Neuroscience*, *15*(4), 487–509. https://doi.org/10.1093/scan/nsaa057

Weiner, K. S., & Grill-Spector, K. (2011). Not one extrastriate body area: Using anatomical landmarks, hMT+, and visual field maps to parcellate limb-selective activations in human

lateral occipitotemporal cortex. *NeuroImage*, *56*(4), 2183–2199. https://doi.org/10.1016/j.neuroimage.2011.03.041

Wurm, M. F., & Erigüç, D. Y. (2025). Decoding the physics of observed actions in the human brain. *eLife*, *13*. https://doi.org/10.7554/elife.98521.3

Xia, M., Wang, J., & He, Y. (2013). BrainNet Viewer: a network visualization tool for human brain connectomics. *PLoS ONE*, *8*(7), e68910. https://doi.org/10.1371/journal.pone.0068910

Xue, S. W., Weng, X. C., He, S., & Li, D. W. (2013). Similarity representation of pattern-information fMRI. *Chinese Science Bulletin*, *58*(11), 1236–1242. https://doi.org/10.1007/s11434-013-5743-0

Ziccarelli, S., Errante, A., & Fogassi, L. (2024). Direction and velocity kinematic features of point-light displays grasping actions are differentially coded within the action observation network. *NeuroImage*, 120939. https://doi.org/10.1016/j.neuroimage.2024.120939